

PAPER • OPEN ACCESS

A non-symmetric Gaussian wake model for lateral wake-to-wake interactions

To cite this article: A Vad *et al* 2023 *J. Phys.: Conf. Ser.* **2505** 012046

View the [article online](#) for updates and enhancements.



Connect with decision-makers at ECS

Accelerate sales with ECS exhibits, sponsorships, and advertising!

▶ Learn more and engage at the 244th ECS Meeting!

A non-symmetric Gaussian wake model for lateral wake-to-wake interactions

A Vad, S Tamaro, C L Bottasso

Wind Energy Institute, Technical University of Munich, Boltzmannstraße 15, D-85748 Garching bei München, Germany

E-Mail: andi.vad@tum.de

Abstract. In this paper, we propose a new non-symmetric Gaussian wake model, which allows for different lateral expansions on the two sides of a wake to account for its interaction with neighbouring wakes. The proposed model is formulated following classical speed-deficit assumptions and momentum conservation. Departing from the existing literature, a non-symmetric Gaussian function is used to represent the velocity deficit in the wake. Accordingly, different wake expansions are assumed on the two sides of the wake, each expressed as a function of the locally prevailing turbulence intensity. The model considers that wake-added turbulence changes with downstream distance; hence, the turbulence intensity on a wake-immersed side of the wake is location dependent. The new model is compared to LES-ALM numerical simulations of three turbines in partial wake overlap. The free parameters of the model describing the wake development are tuned based on the CFD results. Results indicate that the new model provides for a very good agreement of the velocity profiles at different downstream positions, generating an improved representation of merging wakes and their downstream development.

1. Introduction

Analytical (engineering) wake models are indispensable for computing-intensive or time-critical applications, such as wind farm design and control. Over time, these wake models are being continuously improved to capture more of the complex flow phenomena that result from the interaction of wind turbines within a wind farm and from the interaction of the farm with the atmospheric boundary layer [1, 2]. While analytical models can already capture the steady-state characteristics of single fully-developed wakes quite well, there is no common consensus yet on how to model superimposing wakes [3–5]. It is the goal of this paper to contribute filling this gap, by developing a new model for laterally interacting wakes.

It is well known that ambient turbulence (which is strongly linked to atmospheric stability) affects wake recovery [6]. However, in addition to ambient turbulence, the wake itself produces some extra turbulence (termed “wake-added turbulence”) [7]. Hence, the wake released by a wake-affected wind turbine develops under the combined effects of the ambient and of the wake-added turbulence. Every time a downstream turbine is operating in partial wake overlap, it releases behind it a wake that is immersed in the upstream wake on just one of its two sides. When this happens, it is reasonable to expect that the wake expansion will be different on the two sides. In fact, different turbulence intensities, and hence mixing, prevail on each side: one is exposed to the ambient flow, while the other is immersed in the upstream wake. This lack of symmetry between the two sides of a wake is not considered by existing wake models.



In the following, the model equations for the new non-symmetric wake model are first derived. Next, the new model is compared with the original symmetric Gaussian formulation, and both are then contrasted with CFD results, which are assumed as the ground truth.

2. Model derivation

In this work, Bastankhah's velocity model [8] is modified to take into account the influence of a spatially varying turbulence intensity on wake development, as caused by overlaps with wakes released by neighboring turbines. Therefore, a new logic is introduced to calculate the evolution of wakes, which accounts for downstream changes in the flow characteristics in which the wake develops. This differs from the classical model, which on the contrary assumes the same development of the wake on its two lateral sides, and an evolution downstream that only depends on the ambient conditions at the rotor disk of the shedding turbine.

2.1. Velocity model

The Gaussian velocity model of Bastankhah et al. [8] is modified to enable a non-symmetric Gaussian distribution of the velocity deficit. For simplicity, only the equations for the far wake region are modified. To enable different wake expansions on the lateral sides of the wake, the distribution of the velocity deficit is split into two halves, where each half is characterized by a unique standard deviation ($\sigma_{y,l}$ for the left half, $\sigma_{y,r}$ for the right half). The velocity deficit, defined as the ratio of the wake velocity U to the inflow velocity U_∞ , at a specific lateral coordinate y and vertical coordinate z can then be expressed as follows:

$$\frac{U}{U_\infty} = 1 - C \exp\left(\frac{-\Delta y^2}{2\sigma_y^2}\right) \exp\left(\frac{-\Delta z^2}{2\sigma_z^2}\right), \quad (1)$$

$$\sigma_y = \begin{cases} \sigma_{y,l}, & \Delta y \geq 0 \\ \sigma_{y,r}, & \Delta y < 0 \end{cases}, \quad (2)$$

where $\Delta y = y - (y_{WEC} + \delta)$ and $\Delta z = z - z_{WEC}$ are the distances to the centerline of the wake from the hub coordinates $(x_{WEC}, y_{WEC}, z_{WEC})$, while the lateral wake deflection is noted δ . C is the maximum velocity deficit, while σ_y is either equal to $\sigma_{y,r}$ or $\sigma_{y,l}$, depending on which side of the wake the velocity deficit is calculated. This allows for a non-symmetric Gaussian distribution of the velocity deficit in the lateral direction. Following [8], the conservation of momentum deficit is enforced as follows:

$$\frac{d}{dx} \int_{-\infty}^{\infty} \int_{-\infty}^{\infty} U(U_\infty - U) dy dz \approx 0. \quad (3)$$

Considering that the center of the wake is at $y = 0$, this equation can be split into the two lateral sides of the wake:

$$\frac{d}{dx} \int_{-\infty}^{\infty} \int_{-\infty}^0 U(\sigma_{y,l}) [U_\infty - U(\sigma_{y,l})] dy dz + \frac{d}{dx} \int_{-\infty}^{\infty} \int_0^{\infty} U(\sigma_{y,r}) [U_\infty - U(\sigma_{y,r})] dy dz. \quad (4)$$

Inserting (1) into (4) and solving the integral, one obtains:

$$\frac{d}{dx} U_\infty^2 C (2 - C) (\sigma_{y,l} + \sigma_{y,r}) \sigma_z = 0. \quad (5)$$

Assuming that U_∞ is not changing in the direction of the flow, and that the velocity deficit at any downstream position of the far wake is equal to the velocity deficit at its onset, leads to:

$$C_0 (2 - C_0) 2\sigma_{y0} \sigma_{z0} = C (2 - C) (\sigma_{y,l} + \sigma_{y,r}) \sigma_z. \quad (6)$$

There are two solutions for the maximum velocity deficit in the far wake C , the only reasonable one being:

$$C = \frac{-\sqrt{\sigma_z \sigma_{y,sum} (\sigma_z \sigma_{y,sum} + 2\sigma_{z0} \sigma_{y0} C_0^2 - 4\sigma_{z0} \sigma_{y0} C_0)} + \sigma_z \sigma_{y,sum}}{\sigma_z \sigma_{y,sum}}, \quad (7)$$

with $\sigma_{y,sum} = \sigma_{y,l} + \sigma_{y,r}$.

Figure 1 shows an example of how the velocity distribution changes with different standard deviations on the two lateral sides, as caused by different local turbulence intensities; the figure also reports the results for the original symmetric formulation. Note that the total momentum deficit is the same in both cases, and only its lateral distribution differs in the two plots. Due to the higher turbulence on the right side of the wake (right defined looking downwind, in the negative y -direction), the velocity deficit shifts towards this side because of the locally stronger mixing.

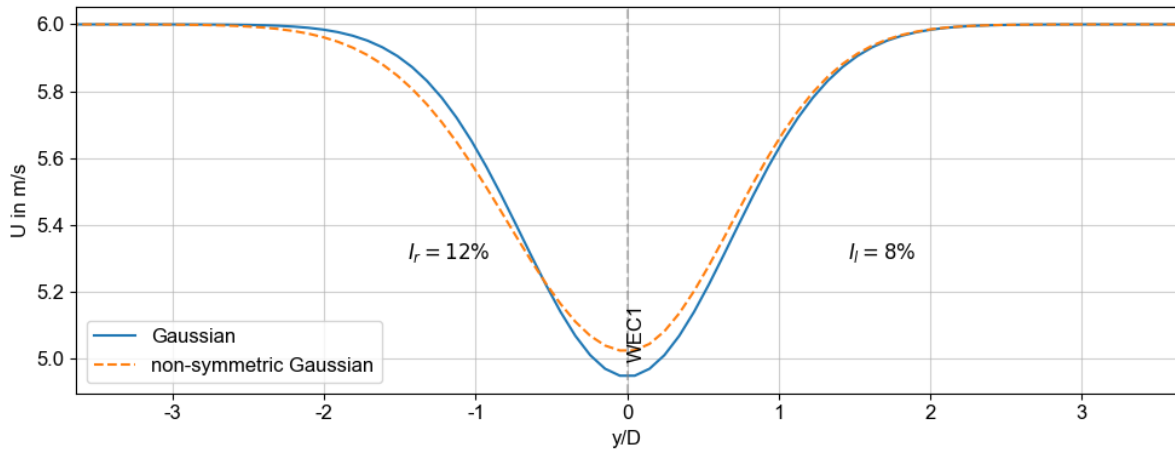


Figure 1: Velocity distributions. Solid line: Gaussian distribution; dashed line: non-symmetric Gaussian distribution with different turbulence intensities on its two sides.

2.1.1. Turbulence model and wake growth

In the classical model, wake growth is typically a function of the local turbulence intensity at the turbine rotor. The local turbulence intensity is formed by the ambient turbulence intensity I_{amb} and the wake-added turbulence intensity I^+ of any upwind turbines, i.e.

$$I_{local} = \sqrt{I_{amb}^2 + rI_+^2}. \quad (8)$$

In Floris v2.4 [9], r is the area overlap of the incoming wake cross-section and the rotor disk of the shaded turbine, i.e. $r = A_{wake}/A_{rotor}$. Since the proposed model requires that the local turbulence intensity can be calculated at any point, the definition of r changes to a simple flag, which indicates if the point, where the turbulence intensity shall be calculated, is in the wake area of an upstream turbine or not:

$$r = \begin{cases} 1, & \text{in the wake,} \\ 0, & \text{not in the wake.} \end{cases} \quad (9)$$

Figures 2 and 3 depict a cluster of two turbines, where the downstream one and its wake are affected on one side by the wake released by the upstream machine. Consequently, the local turbulence intensity at the downstream turbine is greater on the right side of the rotor because this side is in the wake of the upstream turbine ($r = 1$), whereas the other side is in free stream ($r = 0$).

The wake-added turbulence intensity I^+ can be calculated with various models [7, 10, 11]. In this study the formulation of Crespo and Hernandez is used, which writes:

$$I^+ = p_{constant} a^{p_{ai}} I_{amb}^{p_{initial}} \left(\frac{x}{D} \right)^{p_{downstream}}, \quad (10)$$

where $p_{constant}$, p_{ai} , $p_{initial}$ and $p_{downstream}$ are four tunable parameters, while a is the axial induction and D the rotor diameter [7]. For several overlapping wakes, turbulence intensities are combined in a recursive way for all affecting wakes at a specific location:

$$I_{local} = \max \left(I_{local}, \sqrt{I_{local}^2 + I_+^2} \right). \quad (11)$$

Knowing the turbulence intensities on all sides of the wake, the lateral wake growth factors k_r and k_l , as well as the vertical wake growth factor k_z , can be calculated based on the parameters k_a and k_b (cf. figure 2 using I_r, I_l for k_r, k_l and I_m for k_z):

$$k = k_a I_{local} + k_b. \quad (12)$$

In the example displayed in figure 2, the wake growth factor on the right side of the rotor k_r will be greater than the one on the left side k_l , because of the higher local turbulence intensity on this side.

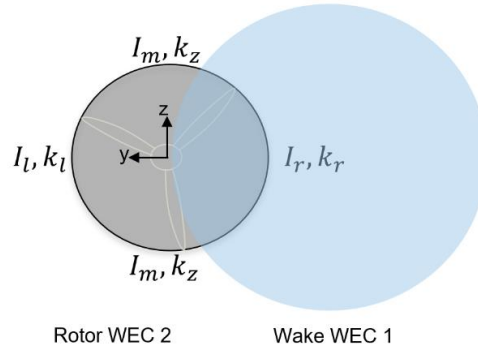


Figure 2: Downwind view of the wake released by the upstream WEC 1 (wind energy converter 1), partially overlapping with the rotor of the downstream WEC 2.

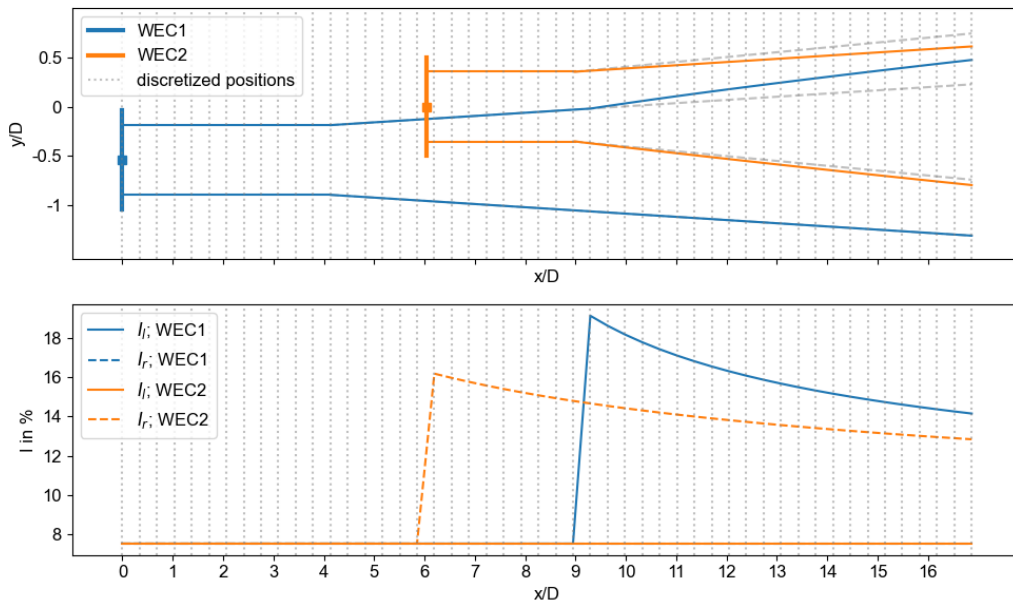


Figure 3: Top: downstream development of the wake boundaries with the new model (expressed as standard deviation of the Gaussian velocity distribution). Bottom: development of turbulence intensity calculated with equations (8-11).

Wake-added turbulence is a function of the streamwise coordinate x , and therefore changes constantly. Additionally, the number of wakes at different downwind positions may vary. Consequently, the wake growth factors must be updated based on the local turbulence intensities along the sides of the wake. To accomplish this, the domain is divided into streamwise sections, and for each section the growth factors of all wakes are updated based on the turbulence intensity prevailing at their lateral sides. In figure 3 the boundaries of the sections are indicated by the grey dotted lines. Behind the near-wake region (shown as horizontal lines behind the rotor), the far wake expands laterally in each section with a wake growth factor that depends on the local turbulence intensity at the respective lateral side according to equation (12). The streamwise development of the local turbulence intensity at the lateral sides of the wakes is shown in the lower subplot of figure 3. In this case, the left side of the wake shed by WEC 1 is only affected by the wake released by WEC 2 behind the onset of its far wake (notice that, while turbulence intensity does increase in the near wake (cf. Figure 4), only the far-wake-added turbulence is considered here; the complex flow phenomena taking place in the near wake are out of the scope of the present work, and deserve dedicated studies.). As the turbulence intensity decreases downstream, the wake growth also decreases when moving downstream. The wake growth calculated with the classical symmetric Gaussian model is shown for comparison using a dashed grey line.

To calculate the wake expansions $\sigma_{y,r}$ and $\sigma_{y,l}$ at an arbitrary downwind position, the individual wake expansions in each section must be summed up all the way to the requested point, i.e.

$$\sigma_{y,r/l} = \sigma_{y0} + \mathbf{k}_{r/l}^T \mathbf{s} = \sigma_{y0} + \begin{pmatrix} 0 \\ \vdots \\ k_0 \\ k_i \\ \vdots \\ k_{i+n} \\ 0 \\ \vdots \end{pmatrix}^T \begin{pmatrix} 0 \\ \vdots \\ x_i - x_0 \\ x_{i+1} - x_i \\ \vdots \\ x_r - x_{i+n} \\ 0 \\ \vdots \end{pmatrix}, \quad (13)$$

where \mathbf{k}_r and \mathbf{k}_l are the right and left vectors, respectively, of a specific wake containing the growth factors for each one of its streamwise sections. The lengths of each section are stored in vector \mathbf{s} , starting at the end of the near wake and ending at the requested point x_r . \mathbf{s} is therefore a vector of zeros until the onset of the far wake x_0 . From this point on, it stores the lengths of the sections until the requested point, past which it again contains zeros. In order to calculate vector \mathbf{k} , the domain is sampled from front to back, and each individual growth factor is calculated based on the local turbulence intensity (i.e., depending on neighbouring wakes). This ensures that changes in wake growth (and also of neighbouring wakes) are considered in the calculation.

The turbulence intensity at the rotor (I_m) is assumed to be the average between the turbulence on the left and right sides. The wake expansion in the vertical direction is assumed to be linear:

$$\sigma_z = \sigma_{z0} + k_z(x - x_0). \quad (14)$$

Knowing the wake expansions of all wakes at any downwind position through equation (13), the velocity deficit of each wake can be calculated with equation (1) and combined using a suitable wake combination model. Usually either a linear or a squared-root wake superposition is used, although there is no common consensus yet on which combination model yields the best results. In this work the linear wake combination model is employed, as it showed better agreement with field data in previous studies [2, 12]. The length and velocity distribution of the near wake was adopted from [8] and depends on the misalignment γ , on the thrust coefficient C_T , computed with the average wind speed in the rotor area, and on the turbulence intensity I_{local} at the rotor, according to:

$$\frac{x_0}{D} = x_{WEC} + \frac{\cos \gamma (1 + \sqrt{1 - C_T})}{\sqrt{2}(4\alpha I_{local} + 2\beta(1 - \sqrt{1 - C_T}))}. \quad (15)$$

3. Comparison to LES

3.1. LES setup

High-fidelity CFD simulations are used as benchmark to verify and validate the proposed wake model. The CFD software SOWFA used in this work was proven to accurately simulate wake dynamics and wake interactions in previous studies [13, 14]. The domain is discretized using a structured Cartesian mesh consisting of approximately 13.5 million cells. The smallest cells have a size equal to 1 meter, and they are located in the immediate vicinity of the turbine rotors; six levels of coarsening are applied to limit the computational effort. The PISO algorithm [15] is used to handle the velocity-pressure coupling in the Navier-Stokes Equations, and turbulence is modelled with the large eddy simulation approach (LES) using the constant Smagorinsky method to model subgrid scales [16]. The domain consists of a cluster of three IEA 3.4 MW wind turbines [17] operating at a distance of 4 rotor diameters. A partial wake impingement condition is obtained by laterally staggering the wind turbines by half a diameter relatively to the incoming flow. The inflow is obtained from a precursor simulation in neutral atmospheric conditions, and it is characterised by a turbulence intensity of 6 % at hub height, a shear of 0.2, and a mean wind speed of 9.5 m/s. The actuator line method [16] is used to model the blades by directly coupling the LES environment with the aeroservoelastic simulator FAST [18].

Figure 4 shows the average wind speed and turbulence intensity over the simulated area for a period of 4 minutes (with a time step of 0.01s). The partial wake overlaps of WEC 1 and 2 lead to increased turbulence intensities on the affected sides, while the others are immersed in the ambient turbulence. This asymmetric distribution of the turbulence intensity leads to different mixing and thus to a different wake growth on the two sides of the wakes. To analyse this effect, the velocity distributions of the overlapping wakes at four downstream locations in the far wake (marked in the upper subplot in figure 4) are compared with the proposed non-symmetric Gaussian and the classical Gaussian models.

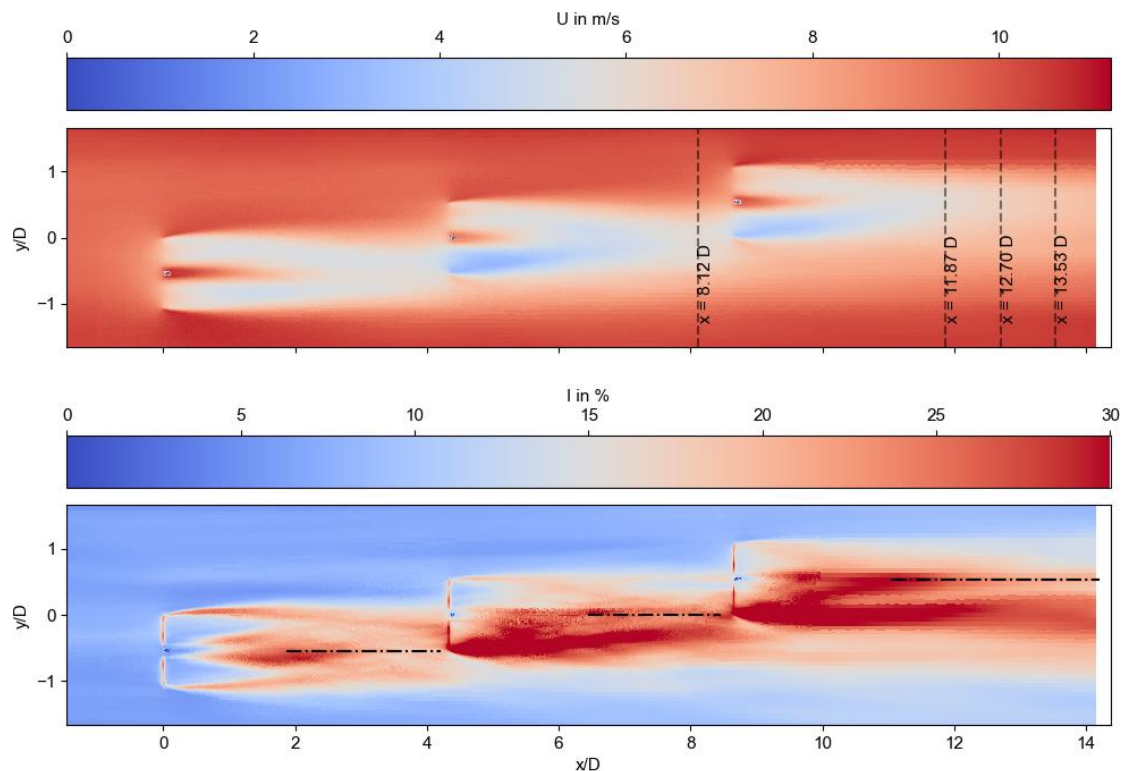


Figure 4: LES flowfields. Top: average velocity flowfield at hub height. Bottom: turbulence intensity flowfield. Planes used to tune the turbulence parameters are indicated with black lines.

3.2. Comparison of turbulence intensity and velocity profiles

Both the Gaussian and the non-symmetric Gaussian models depend on several tunable wake parameters. The parameters can be adjusted by comparing the calculated velocities and turbulence intensities with the LES results, which are taken as ground truth.

First, the turbulence parameters from equation (10) are adjusted to match the turbulence intensity of the LES solution behind the turbines. The turbulence intensities are extracted at the centrelines of the far wakes, as marked in figure 4. The parameters are fitted with the least squares method. Figure 5 plots the fitted curves of the turbulence model against LES. Results indicate a good fit for the development of turbulence intensity behind WEC 1 and 3, and a turbulence intensity of the correct order of magnitude behind WEC 2. The fact that the agreement is worse behind WEC 2 could be caused by the interactions of the two wakes and of the induction zone in front of WEC 3, resulting in a complex flow pattern upstream of the third turbine.

Applying these estimated turbulence parameters to both the Gaussian and non-symmetric Gaussian models, the velocities at the selected downstream positions can be compared. The remaining parameters are kept at the default values recommended in Floris v2.4. Figure 6 shows the overall speed distributions resulting from the lateral wake interactions, for the two models at the four downstream positions (as shown in figure 4). In addition, the figure also shows the individual wakes in dashed lines. Just by adjusting the turbulence parameters, the non-symmetric Gaussian model already seems to achieve a good agreement with the LES results. The non-uniform lateral distribution of the turbulence intensity leads to a larger expansion in the positive y -direction of WEC 1 and 2, while the wake of WEC 3 expands more in the negative y -direction. This is best seen by looking at the upper subplot at $x/D = 13.53$ in figure 6. The non-uniform distribution of the individual wakes leads to a close agreement with the LES velocity profile.

On the other hand, the classical symmetric Gaussian model (lower subplots) underestimates the velocity deficits at all downwind positions. One reason for this could be that the tuned turbulence leads to higher wake-added turbulence intensities, compared to the default model. This leads, in the case of the Gaussian model, to higher wake growth factors on all sides of the wake; on the other hand, for the non-symmetric Gaussian model the wake-added turbulence only affects one side of the wake, resulting in a good agreement with LES.

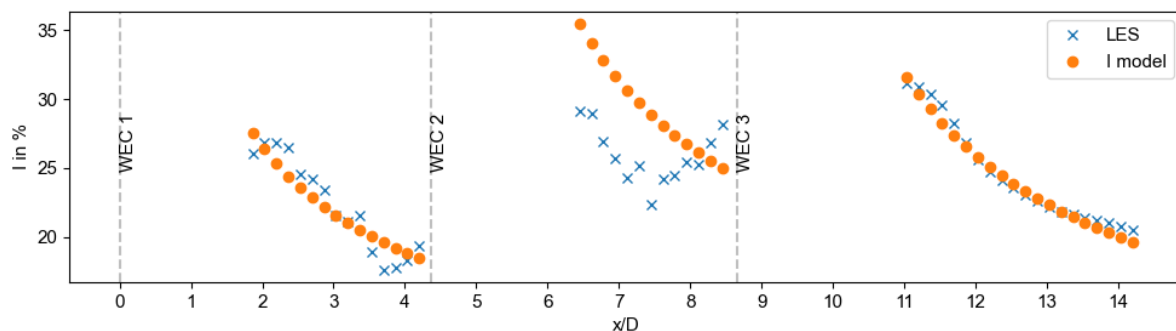


Figure 5: Comparison of the turbulence intensity development behind each rotor between LES and the Crespo Hernandez model.

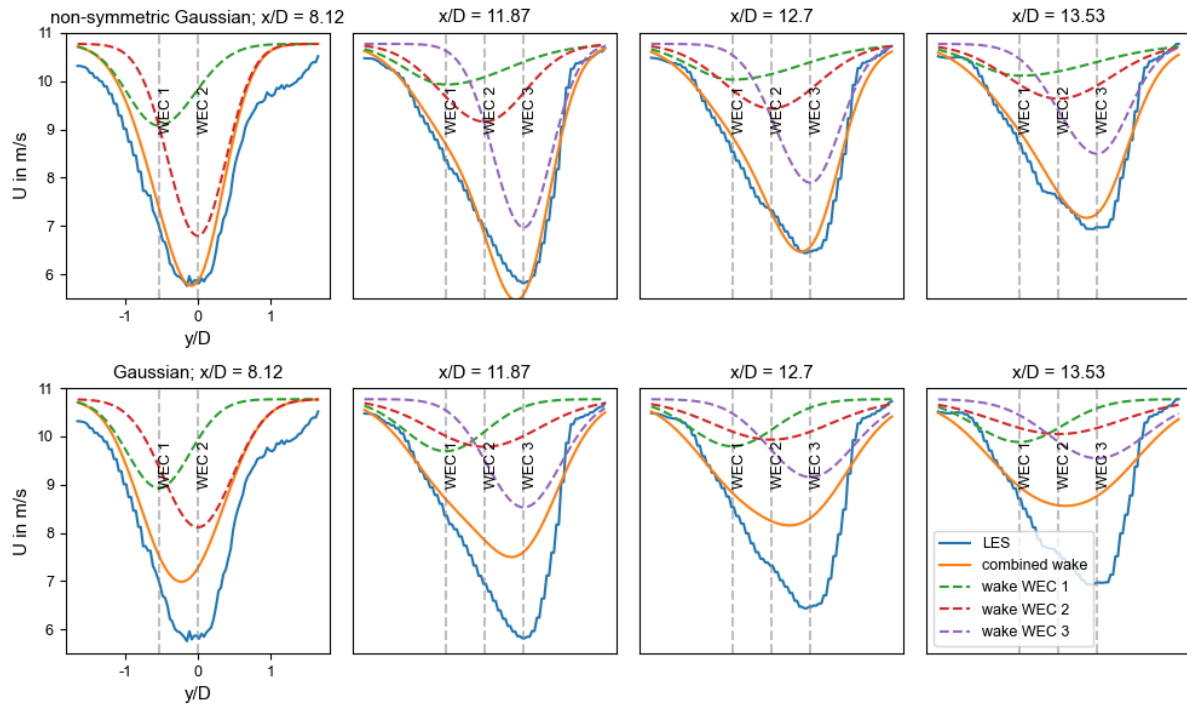


Figure 6: Comparison of the Floris-calculated velocity profiles with LES. Top: non-symmetric Gaussian; bottom: classical symmetric Gaussian model. Dashed lines represent the individual wakes computed by Floris.

By fitting the turbulence parameters to LES, a better description of the actual wake-added turbulence was achieved. Since the new parameters differ from the standard one, the effect of the velocity parameters, which depend on turbulence intensity, also changes. To investigate how the velocity parameters change with the new turbulence parameter values, parameters k_a , k_b , α and β are tuned to the LES velocity profiles. The parameters k_a and k_b are responsible for the wake growth (see equation (12)), while parameters α and β are responsible for the length of the near wake according to equation (15). A global multivariate optimisation is performed using the Differential Evolution solver [19]. The Root Mean Square (RMS) error of the velocity deficits at the four positions marked in figure 4 is used as the cost function.

Table 1 lists the identified velocity parameters for the two models. For the non-symmetric Gaussian model, the parameters are not significantly changed by tuning, as the model already showed a good agreement with LES even with the default values. For the Gaussian model, however, the identified parameters considerably deviate from the standard values. Figure 7 shows the resulting velocity deficit at $x/D = 13.53$ for both tuned models. The figure shows that both models achieve a good fit with the LES reference, but in different ways. In fact, the symmetric Gaussian model achieves a good fit by changing the wake velocity parameters so that the wake expansions are smaller and the maximum wake deficits greater. This is accomplished by a smaller k_a and thus smaller wake growth and a longer near wake region (smaller α). The non-symmetric Gaussian, on the other hand, achieves a good fit through the asymmetric distribution of the individual wakes, and much less so through the tuning of the velocity parameters. According to the LES velocity profiles, the end of the near wake behind WEC 1 is expected to be between 4 and 5 D . For the Gaussian model, the near wake ends at 6.5 D when the tuned parameters are used (i.e., unrealistically further downstream), whereas for the new non-symmetric Gaussian it is located close to the expected position at 5.1 D . This, together with the fact that the new non-symmetric model achieves a very good agreement with LES even without the tuning of velocity

parameters, strongly suggests that its representation of lateral wake interactions is more physically meaningful than the one provided by the symmetric approach.

	k_a	k_b	α	β
Initial	0.38	0.004	0.58	0.077
Gaussian	0.07	0.030	0.42	0.11
Non-symmetric Gaussian	0.34	0.001	0.63	0.093

Table 1: Wake velocity parameters.

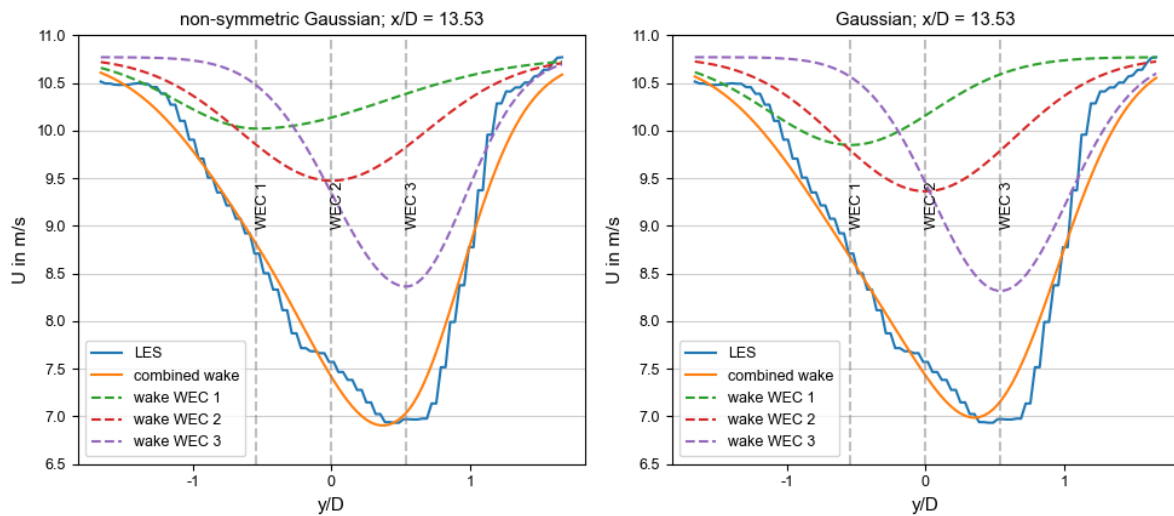


Figure 7: Comparison of the tuned Gaussian and non-symmetric Gaussian models with LES at $x/D = 13.53$.

4. Conclusion and outlook

In this work, a new non-symmetric Gaussian wake model was formulated, which allows for different lateral expansions on the two sides of a wake, in accordance with the local turbulence intensity. This enables taking into account the presence of laterally interacting wakes. In addition, the model also considers that turbulence intensity evolves when moving downstream inside a wake, which further affects the development of a neighbouring wake. The increased complexity of the new model comes at the expense of an increased computational cost. To calculate the flow field of the three interacting turbines, the proposed model takes about four times longer than Floris v2.4. However, this drawback can be more than compensated with an increase in accuracy considering that it is still by order of magnitudes faster than medium- or high-fidelity models like RANS or LES.

The new model as well as the classical symmetric Gaussian formulation are compared with a LES simulation of three turbines operating in partial wake overlap. After fitting the turbulence parameters of the Crespo Hernandez turbulence model to the LES results, the proposed model generates an overall velocity profile resulting from the lateral interaction of the wakes that is in a very good agreement with the numerical simulation, unlike the Gaussian model. Further tuning of the velocity parameters leads to good matches for both models with respect to LES. However, the velocity parameters of the Gaussian model deviate strongly from the default values, suggesting overfitting. In other words, the match is good because there are enough degrees of freedom in the model to generate the desired profile, but the resulting parameters take unphysical values.

The current study is limited to one specific scenario, and therefore it is clear that further analyses are needed to confirm the findings reported here, and to gain a more detailed insight into the performance of the proposed method. Future work will also compare the model with scaled experimental and full-

scale field data. In particular, the downstream adjustment of wake growth that is included in the proposed model seems especially promising when dealing with deep array effects, where many wakes can undergo significant simultaneous lateral interactions. Additionally, the model can be extended to allow variable wake growth also in the vertical direction, for example to include effects due to the ground or caused by the interaction with the atmospheric boundary layer. Further improvements are possible by refining the description of the near wake region. For this purpose, the symmetric double Gaussian formulation of [20, 21] can be extended to a non-symmetric double Gaussian one, to account for different recoveries on the lateral sides of the near wake due to partial wake overlaps.

Acknowledgements

This work is funded in part by the European Union under the Horizon Europe grant No. 101084216 (project MERIDIONAL). Moreover, the authors would like to thank the Leibniz Supercomputing Centre (LRZ) for providing access and computing time on the SuperMUC Petascale System under Projekt-ID pr84be “Large-eddy Simulation for Wind Farm Control”.

Appendix

	$p_{constant}$	p_{ai}	$p_{initial}$	$p_{downstream}$
Initial value	0.73	0.83	-0.0325	-0.32
Fitted value	1.17	0.49	0.06	-0.55

Table A1: Wake turbulence parameters.

	x_0/D WEC 1	x_0/D WEC 2	x_0/D WEC 3
LES (estimate)	Between 4 and 5	Between 6.5 and 7.5	Between 10.5 and 11.5
Gaussian	6.5	6.8	10.6
Non-symmetric Gaussian	5.1	6.8	10.8

Table A2: Locations where the near wake ends.

References

- [1] Doekemeijer B M, Simley E and Fleming P 2022 *Energies* **15** 1964
- [2] Hamilton N, Bay C J, Fleming P, King J and Martínez-Tossas L A 2020 *Journal of Renewable and Sustainable Energy* **12** 53311
- [3] Bastankhah M, Welch B L, Martínez-Tossas L A, King J and Fleming P 2021 *J. Fluid Mech.* **911**
- [4] Howland M F and Dabiri J O 2021 *Energies* **14** 52
- [5] Vogel C R and Willden R H J 2020 *Wind Energ.* **23** 593–607
- [6] Abkar M and Porté-Agel F 2015 *Physics of Fluids* **27** 35104
- [7] Crespo A and Hernández J 1996 *Journal of Wind Engineering and Industrial Aerodynamics* **61** 71–85
- [8] Bastankhah M and Porté-Agel F 2016 *J. Fluid Mech.* **806** 506–41
- [9] NREL 2021 FLORIS. Version 2.4.0 *GitHub repository* (GitHub) <https://github.com/NREL/floris>
- [10] Frandsen S 2007 *Turbulence and turbulence-generated structural loading in wind turbine clusters (Risø-R 1118 (EN))* (Risø DTU - National Laboratory for Sustainable Energy; available from: Risø National Laboratory, Information Service Department)
- [11] Ishihara T and Qian G-W 2018 *Journal of Wind Engineering and Industrial Aerodynamics* **177** 275–92
- [12] Braunbehrens R, Vad A and Bottasso C L 2022 *The wind farm as a sensor: learning and explaining orographic and plant-induced flow heterogeneities from operational data*
- [13] Wang J, Wang C, Campagnolo F and Bottasso C L 2019 *Wind Energ. Sci.* **4** 71–88
- [14] Wang J, Wang C, Campagnolo F and Bottasso C L 2018 *A Large-Eddy Simulation Approach for Wind Turbine Wakes and its Verification with Wind Tunnel Measurements*
- [15] Issa R 1986 *Journal of Computational Physics* **62** 40–65

- [16] Meneveau C 2006 *Large Eddy Simulation for Incompressible Flows: An Introduction (Scientific Computation Ser)* 3rd edn (Berlin, Heidelberg: Springer Berlin / Heidelberg)
- [17] Bortolotti P, Tarres H C, Dykes K L, Merz K, Sethuraman L, Verelst D and Zahle F 2019 *IEA Wind TCP Task 37: Systems Engineering in Wind Energy - WP2.1 Reference Wind Turbines*
- [18] Jonkman J M and Buhl M L JR. 2005 *FAST User's Guide - Updated August 2005*
- [19] Storn R and Price K 1997 *Journal of Global Optimization* **11** 341–59
- [20] Schreiber J, Balbaa A and Bottasso C L 2020 *Wind Energ. Sci.* **5** 237–44
- [21] Soesanto Q M B, Yoshinaga T and Iida A 2022 *Energy Science & Engineering* **10** 2123–45